

X-ray emissions in $3d$, $4d$, and $5d$ ranges for uranium ions

C. Bonnelle, P. Jonnard, C. Barré, and G. Giorgi

Laboratoire de Chimie Physique Matière et Rayonnement, URA 176, Université Pierre et Marie Curie, 11 rue Pierre et Marie Curie, 75231 Paris Cedex, France

J. Bruneau

CEA, Centre d'Etude de Limeil-Valenton, Boîte Postale 15, 94195 Villeneuve-Saint-Georges Cedex, France

(Received 28 October 1996)

Radiative decay of $nd^{-1}5f^{m+1}$ excited states in UO_2 induced by electron collisions is studied theoretically and experimentally. Energies, transition probabilities, and photoexcitation cross sections for the relevant configurations of U^{4+} are calculated by using the multiconfiguration Dirac-Fock method. Experimental observations are made in the $4d$ range. Direct recombination of the excited $5f$ electron to the $4d$ hole and $4d-6p$ emission in the presence of the spectator excited $5f$ electron are observed. From the theoretical results, the spectra are simulated and compared to the observed spectra in the three nd regions. The agreement is correct and describes the evolution of the coupling scheme in the $nd^{-1}5f^3$ excited states from $n=3$ to $n=5$. [S1050-2947(97)00605-7]

PACS number(s): 32.70.-n, 31.50.+w

I. INTRODUCTION

Dynamics of the *excited x-ray states*, i.e., excited states with a core hole, can be studied from their decay processes. Indeed the observation of the *resonant X emissions*, which correspond to the radiative recombination of the excited electron to the core hole, is a direct method to characterize the highly excited states present in a material. First identification of excited x-ray states were made in emission [1] and Auger [2] $3d$ spectra of solid lanthanides. Then the different processes possible from lanthanide nd^9 ($n=3,4$) $4f^{m+1}$ excited states were identified. They are of two types, resonant transitions [3–9] and transitions in the presence of the spectator excited electron [3,10].

In the actinides, the presence of nd^95f^{m+1} excited states was established by the observation of resonant X emissions in the $3d$ spectra of Th, U, and Pu [11,12] and in the $5d$ spectra of Th and U [13], both in the metal and the oxide. These emissions are less intense than those of the lanthanides and their observation is more difficult. In the $3d$ range, the lifetimes of the core hole and of the excited X state are very short and this reduces the spectral resolution. In the $5d$ range, observations were made with very large self-absorption and the shape of the spectra is strongly disturbed.

We present here an analysis of the U $4d$ emission spectrum in uranium dioxide. From this study, we have verified that U $4d^{-1}5f^{m+1}$ quasilocalized excited states are present and decay by the same processes as the $nd^{-1}4f^{m+1}$ ones in the lanthanides, i.e., by resonant emission and emission in the presence of a spectator excited electron. From the experimental data obtained in the $3d$ [11], $4d$ (this work), and $5d$ [13] ranges and from the corresponding calculated emission and photoexcitation spectra, we compare the dynamics of U $nd^{-1}5f^{m+1}$ excited states. We show that there is an analogy between the U $3d$ and $4d$ spectra, where the nd spin orbit is the dominant interaction and whose characteristics are close to those of the lanthanide $3d$ spectra. In contrast the

U $5d$ spectrum is dominated by the $5d-5f$ interaction as in the lanthanide $4d$ spectra.

In our experiments, excited x-ray states are created by collision with incident electrons of energy higher than the threshold energy. Unlike the resonance x-ray scattering [14], the direct radiative decay is independent of the excitation process and collisional excitation–radiative decay can be treated as a two-step process [15,16]. On the other hand, electron collisions induce both transitions from excited and ionized states. Previously, the identification of the resonant X emissions was made by comparing the emission and photoabsorption spectra. Indeed, the resonant X emissions are the reverse process of the photoexcitation and are in coincidence with the photoexcitation lines. Here we identify the transitions from excited X states in the following way: the spectrum is induced with electrons having incident energy E_0 between some eV above the threshold energy and 1.6 times this energy. For each E_0 value, the intensity of the emission from the excited state is compared to that of an emission from the ionized state, labeled *normal* atomic emission. The behavior of the intensity with respect to E_0 serves to identify the two emissions. This method is convenient because it does not require the observation of the photoexcitation spectrum and it can easily be generalized to complex materials.

Calculations are performed in order to determine the energies and the transition probabilities of the resonant $4d$ emissions and of the normal atomic lines that are present in the same energy range. The multiconfiguration Dirac-Fock (MCDF) method is used. Uranium is tetravalent in UO_2 . Four electrons are present in the valence band and partially delocalized in the solid. U^{4+} ions, whose ground configuration is $5f^2$, are present at the lattice nodes. We have calculated the energies and the probabilities of all the normal emissions taking place from $\text{U}^{5+} nl^{-1}5f^2$ with $n=4$. Comparison between the experimental and calculated spectra of the $4d-5p$ emission has been made to test the precision of the theoretical model and also the influence of the multiplet

splitting on the shape of the emission.

In analogy with the transitions between inner subshells, the resonant emissions take place between two discrete states and are quasiatomic in solids. Thus the atomic model is adapted to describe them [17,18]. From U $4d^{-1}5f^{m+1}$ excited states, two emissions have been observed: the resonant $4d_{5/2}$ one and the $4d_{3/2}$ - $6p$ one in the presence of the spectator excited $5f$ electron. Their identification is made by comparing the intensities measured for both transitions and for the $4d_{5/2}$ - $5p_{3/2}$ normal emission as a function of incident electron energy.

In Sec. II, we present our theoretical calculations for the $n=4$ normal (electric dipole) atomic emissions, the nd ($n=3,4,5$) resonant emissions and the $6p$ - nd emissions in the presence of a spectator $5f$ electron. To discuss the relative contribution of excitation and ionization, we have compared the cross sections of both processes. In Sec. III, the experimental characteristics of the $4d$ - $5p$ normal emission, the resonant $4d_{5/2}$ emission, and the $4d_{3/2}$ - $6p$ emissions in the presence of a spectator $5f$ electron are presented and discussed by comparison with the calculated spectrum. Interpretations are justified from the measurement of their relative intensities at different incident electron energies. In Sec. IV, we compare the characteristics of the $n=3,4,5$ excited states and their radiative decay.

II. CALCULATED X-RAY SPECTRA

A. Methodology

The spectra are calculated by using the method described in Ref. [13]. Wave functions and energies are computed with a MCDF program [19]. The initial and final states of the transitions are obtained from the extended average level extension of the MCDF method coupled with the Slater transition state [20]. The length form of the transition matrix elements is used. The average energy of each configuration is the barycenter of all the J levels of the configuration.

For the electric dipole emissions taking place in U^{5+} and in U^{4+} ions with an excited electron, we assume that all the J levels of the initial configuration are populated statistically and we calculate the weighted sum of all the lines associated with the considered transition. Each line is simulated by folding the theoretical probability with a Lorentzian broadening function whose width results from the intrinsic lifetime and the finite experimental resolution.

The $nd \rightarrow 5f$ photoexcitation spectra are obtained by summing all the electric dipole lines from the ground level of the initial configuration ($U^{4+} 5f^2 3H_4$). Each line is fitted by a Lorentzian curve whose surface is equal to the excitation cross section. For the resonant emissions, we have also calculated the radiative recombination from the levels of the $U^{4+} nd^9 5f^3$ excited configuration with $J=3,4,5$ only to the ground state $3H_4$ of $U^{4+} 5f^2$. The photoionization cross section is determined by calculating the free wave function as described in [19].

B. Ionization energies of U^{4+}

In a single MCDF run, the energies of the ground state of $U^{4+} 5f^2 3H_4$ and all the states of U^{5+} with a hole in the n

TABLE I. Ionization energies (eV): (1) calculated for $U^{4+} 5f^2$; (2) calculated for neutral U $5f^3 6d^1 7s^2$ [21]; (3) difference (1)–(2); (4) obtained from UO_2 XPS [22]; (5) deduced from UO_2 x-ray spectroscopy [24,25]; (6) difference (1)–(5).

	(1)	(2)	(3)	(4)	(5)	(6)
$4s_{1/2}^1 5f^2$	1492.0	1478.2	13.8	1444	1443.5	48.5
$4p_{1/2}^1 5f^2$	1325.0	1311.4	13.6	1276	1275.5	49.5
$4p_{3/2}^3 5f^2$	1092.7	1075.9	16.8	1048	1047.5	45.2
$4d_{3/2}^3 5f^2$	826.8	809.1	17.7	783	783.7	43.1
$4d_{5/2}^5 5f^2$	784.1	765.5	18.6	741	742.0	42.1
$4f_{5/2}^5 5f^2$	433.0	413.7	19.3	395	393.5	39.5
$4f_{7/2}^7 5f^2$	421.9	402.5	19.4	384	383.5	38.4
$5s_{1/2}^1 5f^2$	370.0	342.7	27.3	327	329	41.0
$5p_{1/2}^1 5f^2$	303.1	275.6	27.5	262	263	40.1
$5p_{3/2}^3 5f^2$	249.0	220.2	28.8	198	198.7	50.3
$5d_{3/2}^3 5f^2$	149.7	118.4	31.3	108	107.5	42.2
$5d_{5/2}^5 5f^2$	138.9	110.0	28.9	99	100.6	38.3
$6s_{1/2}^1 5f^2$	91.6	58.2	33.4	74	75.1	16.5
$6p_{1/2}^1 5f^2$	69.7	36.5	33.2	45		
$6p_{3/2}^3 5f^2$	59.4	26.8	32.6	35		
$5f_{7/2}^1$	41.1					
$5f_{5/2}^1$	40.4					

=4, 5, or 6 shell are computed. Since the number of the J levels of each state is large, we present in Table I, column (1) only the barycenters of the ionization energies from the ground state of U^{4+} for each subshell. These energies are relative to the vacuum level. We have also given in column (2) the energies obtained by Desclaux [21] for the neutral atom of configuration $5f^3 6d^1 7s^2$. The difference $\Delta[(1) - (2)]$ between the ionization energies calculated for U^{4+} and for neutral U [column (3)] increases with the quantum number of the subshell. Outer orbitals are more sensitive to the loss of the four external electrons than inner ones.

The ionization energies of various subshells have been determined experimentally. Various experimental methods have been used. A well-known direct method is x-ray photoelectron spectrometry (XPS). The precision is a function of the photoelectron energy and the surface state of the sample. The energies determined by Siegbahn *et al.* [22] for oxidized uranium relative to the vacuum level are given in column (4). X-ray spectrometry is also largely used [23]. Indeed, from x-ray emissions observed in some spectral range, the energy differences between the subshells are determined with a large precision. If the energy of a reference subshell is known from XPS or x-ray photoabsorption measurement, the energies of all other subshells can be deduced. The ionization energies of uranium in UO_2 have been determined in this manner from an experimental study of the M emission spectra of uranium [24]. The reference subshell is U $3p_{3/2}$; its energy in UO_2 has been determined by photoabsorption [25]. The energies relative to the vacuum level are given in Table I, column 5 and the differences $\Delta[(1) - (5)]$ between calculated and experimental ionization energies in column 6. These differences decrease slowly with the ionization energy except for the $5p_{3/2}$ and $6s_{1/2}$ subshell. These two cases are discussed in the next section.

TABLE II. Energies (eV) of $U^{4+} 5f^2$ normal N shell emissions: E_{calc} is deduced from ionization energies calculated for $U^{4+} 5f^2$; E_{expt} from UO_2 x-ray spectroscopy ionization energies.

	E_{calc}	E_{expt}	$\Delta(E_{\text{calc}} - E_{\text{expt}})$
$4s_{1/2}-4p_{1/2}$	166.9	168.0	-1.1
$4s_{1/2}-4p_{3/2}$	399.2	400.0	-0.8
$4s_{1/2}-5p_{1/2}$	1188.9	1184.5	+4.4
$4s_{1/2}-5p_{3/2}$	1243.0	1248.8	-5.8
$4s_{1/2}-6p_{1/2}$	1422.2		
$4s_{1/2}-6p_{3/2}$	1432.6		
$4p_{1/2}-4d_{3/2}$	498.3	491.8	+6.5
$4p_{1/2}-5s_{1/2}$	955.1	946.5	+8.6
$4p_{1/2}-5d_{3/2}$	1175.4	1168.0	+7.4
$4p_{1/2}-6s_{1/2}$	1233.4	1200.4	+33.0
$4p_{3/2}-4d_{3/2}$	266.0	263.8	+2.2
$4p_{3/2}-4d_{5/2}$	308.6	305.5	+3.1
$4p_{3/2}-5s_{1/2}$	722.8	718.5	+4.3
$4p_{3/2}-5d_{3/2}$	943.0	940.0	+3.0
$4p_{3/2}-5d_{5/2}$	953.8	946.9	+6.9
$4p_{3/2}-6s_{1/2}$	1001.1	972.4	+28.7
$4d_{3/2}-4f_{5/2}$	393.7	390.2	+3.5
$4d_{3/2}-5p_{1/2}$	523.7	520.7	+3.0
$4d_{3/2}-5p_{3/2}$	577.8	585.0	-7.2
$4d_{3/2}-6p_{1/2}$	757.1		
$4d_{3/2}-6p_{3/2}$	767.4		
$4d_{5/2}-4f_{5/2}$	351.1	348.5	+2.6
$4d_{5/2}-4f_{7/2}$	362.2	358.5	+3.7
$4d_{5/2}-5p_{3/2}$	535.1	543.3	-8.2
$4d_{5/2}-6p_{3/2}$	724.7		
$4f_{5/2}-5d_{3/2}$	283.4	286	-2.6
$4f_{5/2}-5d_{5/2}$	294.1	292.9	+1.2
$4f_{7/2}-5d_{5/2}$	283.0	282.9	+0.1

C. Energies of U^{5+} normal N shell emissions

The average energy of the $n'l'j' \rightarrow nlj$ emission of U^{5+} is estimated as the difference between the barycenters of the U^{5+} free ion with a hole in the nlj or $n'l'j'$ core subshell. The average energies of electric dipole N shell emissions between normally closed subshells are presented in Table II, column 1. The energy of an x-ray emission can also be predicted from the difference between the experimental ionization energies of the two subshells. We have given in Table II, column 2 the energies of N shell emissions obtained from experimental ionization energies and in column 3 the differences between these values and the calculated energies. Theoretical values of the emission energies generally are higher than the experimental ones by a few eV. We note two anomalies, the first in the position of $6s$ level, the second in the $5p$ relativistic splitting.

For $4p_{1/2}-6s$ and $4p_{3/2}-6s$ emissions, the differences between the theoretical and experimental energies are +33.0 and +28.7 eV, respectively. If we adopt as the experimental energy the value determined for $6s$ subshell of the metal (46.9 eV) [26], these differences reduce to only +4.8 and +0.5 eV. This change cannot be explained by a solid effect. Actually, the physicochemical state changes the energy of the emissions between core subshells by only a few eV. We

suggest that an error is present in the experimental determination of oxide $6s$ ionization energy, increasing the value obtained for the metal by 28 eV.

On the other hand, ΔE is <0 for the lines to $5p_{3/2}$. The calculated $5p_{1/2}-5p_{3/2}$ spin-orbit splitting ($\Delta E_{\text{SO}}=54.1$ eV) is clearly smaller than the experimental value ($\Delta E'_{\text{SO}}=64.3$ eV). This difference is due to the large energy predicted for $5p_{3/2}$ ionization. For the other subshells, calculated and experimental spin-orbit splittings are in agreement and the energies of x-ray emissions are predicted with a precision of some eV.

D. Simulation of U^{5+} normal N shell emissions

Each $n'l'j' \rightarrow nlj$ normal N shell emission is simulated from separated run. This can lead to differences of 1–2 eV in the transition energies when they are compared to those of the previous section, principally because interactions with the other subshells are not taken into account. But this is the simpler way to compute the transition rates with the MCDF program when the number of lines between two groups of J levels can reach 5568. The results are indicated in Table III.

As expected, the probability of $4l \rightarrow n(l+1)$ transitions decreases when n increases. For the $4p$ and $4d$ subshells, the spin-orbit splittings are 232 and 42 eV, respectively, and provide well-separated emissions. The transition probability ratios of various spin-orbit components are clearly different from their statistical weights. For the $4p_{3/2}-4d$ to $4p_{1/2}-4d$ and $4p_{3/2}-5d$ to $4p_{1/2}-5d$ transitions, the ratios are, respectively, 0.27 and 3.9 while their expected value is 2. This could be attributed to the difference between the relativistic $j=l-\frac{1}{2}$ and $j=l+\frac{1}{2}$ orbitals.

The strong interaction between the $5d$ and $5f$ subshells widens the $4p_{3/2}-5d$ and $4p_{1/2}-5d$ emission arrays that have numerous structures spread on about 40 eV. In particular, the $5d_{3/2}^{-1}$ state is two times more spread than the others. The sum of transition probabilities P_{tot} , radiative life-times τ , and widths Γ of each $n=4$ subshell are given in Table IV. The electric dipole emissions to $4p$ are twice as intense as those to $4d$.

As an example, we have drawn in Fig. 1 the calculated $U^{5+} 4d-5p$ emission probabilities versus energy. The initial states, $4d_{5/2}^5 5f^2$ and $4d_{3/2}^3 5f^2$, have 62 and 45 J levels respectively, a spread of about 6 eV and are separated by 42.7 eV. The final states, $5p_{3/2}^3 5f^2$ and $5p_{1/2}^1 5f^2$, have 45 and 24 J levels, respectively, a spread of about 5–6 eV and are separated by 54.1 eV. The spectrum is formed by 2976 lines. The three peaks situated around 522, 535, and 577 eV correspond to the $4d_{3/2}-5p_{1/2}$, $4d_{5/2}-5p_{3/2}$, and $4d_{3/2}-5p_{3/2}$ transitions. As expected, the last one with $\Delta J=0$ is clearly less probable than the $\Delta J=1$ transitions.

E. $U^{4+} 5f^2 \rightarrow nd^9 5f^3$ excitation

We have calculated the oscillator strengths corresponding to the photoexcitation of an nd ($n=3,4,5$) electron belonging to the ground configuration $U^{4+} 5f^2$ to the open $5f$ subshell (Table V); the cross sections are plotted in Fig. 2. There are 176 excitation lines in each graph. We have used for the width of each Lorentzian line 3 eV for the $n=3$ spectrum, 1

TABLE III. Energy (eV), transition probability (sec^{-1}), and ratio of spin-orbit component probability for $\text{U}^{4+} 5f^2$ normal N shell emissions, deduced from the calculated spectra.

Final states	E (eV)	P (10^{10} sec^{-1})	E (eV)	P (10^{10} sec^{-1})	
					$4s_{1/2}$
$4p^5 5f^2$			167.1	504	
			398.6		
$5p^5 5f^2$			1190.9	392	
			1244.5		
$6p^5 5f^2$			1430.3	99	
			1440.1		
		$4p_{3/2}$		$4p_{1/2}$	$P_{4p_{3/2}}/P_{4p_{1/2}}$
$4d^9 5f^2$	266.1	250	497.8	937	0.27
	308.6				
$5d^9 5f^2$	944.2	244	1176.7	62	3.9
	955.0				
$5s^1 5f^2$	720.3	313	952.7	220	1.4
$6s^1 5f^2$	998.7	74	1231.1	56	1.3
		$4d_{5/2}$		$4d_{3/2}$	$P_{4d_{5/2}}/P_{4d_{3/2}}$
$4f^{13} 5f^2$	351.4	343	394.1	425	0.8
	362.5				
$5f^1$	737.2	19	780.7	19	1.0
$5p^5 5f^2$	534.1	99	522.9	144	0.7
			576.8		
$6p^5 5f^2$	725.4	17	757.6	26	0.7
			768.1		
		$4f$			
$5d^9 5f^2$	283	17			

eV for $n=4$ spectrum, and 3.4 eV for the $n=5$ one. These values are chosen to enable a comparison with the experimental data.

The $3d$ and $4d$ calculated excitation spectra are similar. In these ranges, the $3(4)d$ spin-orbit splitting predominates the $3(4)d-5f$ interactions and the 176 excitation lines form two well-separated groups of unresolved lines, corresponding to transitions from the $3(4)d_{5/2}$ and $3(4)d_{3/2}$ subshells. The excitation from $3(4)d_{5/2}$ is two to three times stronger than that from $3(4)d_{3/2}$.

The shape of the $5d$ excitation spectrum is clearly different from that of both $3d$ and $4d$ spectra and the average value of the oscillator strength is larger by about 30. The coupling scheme of $5d$ states is far from the pure jj scheme of $3d$ and $4d$ subshells. This redistributes the cross sections towards the high energies. This behavior is similar to the

TABLE IV. Sum of E_1 transition probabilities P_{tot} (sec^{-1}), radiative lifetime τ (sec), and width Γ (eV) of $\text{U}^{4+} 5f^2 n=4$ subshells.

	P_{tot} (10^{10} sec^{-1})	τ (10^{-13} sec)	Γ (10^{-3} eV)
$4s_{1/2}$	1000	1.00	6.6
$4p_{1/2}$	1280	0.78	8.5
$4p_{3/2}$	880	1.14	5.8
$4d_{3/2}$	610	1.6	4.0
$4d_{5/2}$	480	2.1	3.2
$4f_{5/2,7/2}$	17	59	0.1

well-known one observed in the $4d$ excitation of the light lanthanides [3,10].

F. Photoionization

We have calculated the oscillator strength from $\text{U}^{4+} 5f^2 {}^3H_4$ to the continuum at 790 eV, i.e., just above the $\text{U}^{4+} 4d_{5/2}$ ionization potential (Table I). We obtain 0.004/eV. We have verified that the variation of the photoionization cross section is less than 1% in a narrow range around this energy. Then we estimated at ≈ 75 the ratio of the photoexcitation to the photoionization cross sections at the $4d_{5/2}$ threshold.

G. Emissions from $\text{U}^{4+} nd^9 5f^3$ excited configurations

We have calculated the characteristics of the nd resonant emissions and the $nd-6p$ emissions in the presence of a spectator $5f$ electron (cf. Table V). The $nd^9 5f^3$ configuration has 386 J levels that are statistically populated and the direct recombination takes place from all of these levels to the 13 J levels of $5f^2$. The resonant emissions have 1728 lines instead of 176 lines in the excitation from the ground $\text{U}^{4+} 5f^2 {}^3H_4$. Consequently, resonant emission and photoexcitation spectra are different. To illustrate that, we have plotted in Fig. 3 the $5d$ photoexcitation cross section and the resonant emissions obtained from levels of the $5d^9 5f^3$ configuration with the $J=3,4,5$ only and from all the J levels; the shapes of the emissions are different. In contrast, in the $3d$ range, only the ratio of the $d_{5/2}$ and $d_{3/2}$ components

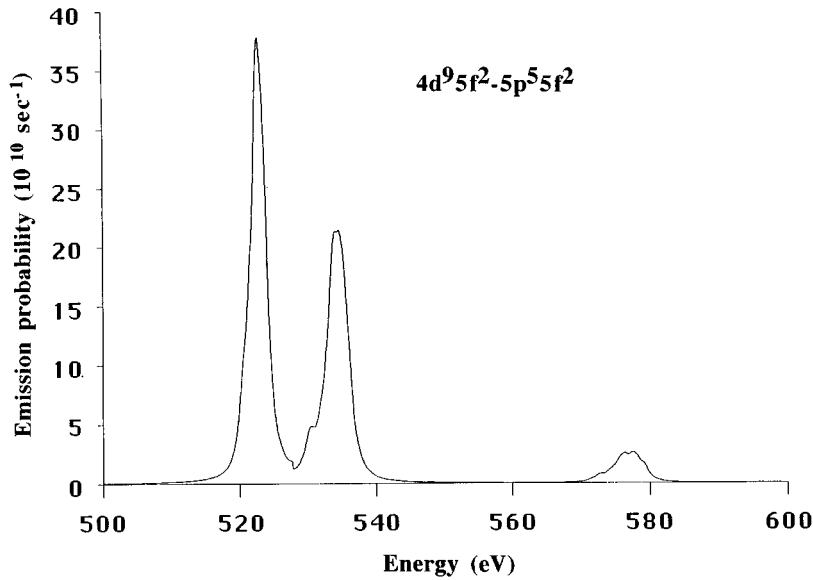


FIG. 1. $U^{5+} 4d^9 5f^2 - 5p^5 5f^2$ calculated emission probability (10^{10} sec^{-1}) with Lorentz 1 eV wide.

changes. As seen in Table V, the $3d_{5/2}$ and $3d_{3/2}$ resonant emissions are in a ratio close to 1 while for the $3d_{5/2}$ and $3d_{3/2}$ oscillator strengths the ratio is 2.3.

In the $4d$ range, the $386 J$ levels of the $nd^9 5f^3$ excited configuration are separated into two subgroups, having 226 and 160 J levels and a spread of about 11 eV. The spin-orbit splitting is 42.4 eV and the ratio of the $d_{5/2}$ and $d_{3/2}$ components is 2.4 times smaller for the resonant emission than for the photoexcitation. The average energy calculated for the $U^{4+} 4d^9 5f^3$ excited states is clearly lower than that of the $U^{5+} 4d^9 5f^2$ states. The difference, ≈ -50 eV, is due to the stabilization of the $5f^3$ configuration and to the screening effect of the $5f$ supplementary electron which decreases the $4d$ subshell energy. The shift between the states $U^{4+} nl^{-1} 5f^3$ and $U^{5+} nl^{-1} 5f^2$ is smaller but of the same order of magnitude. Then the emissions from $U^{4+} 4d^9 5f^3$ are shifted with respect to the emissions from $U^{5+} 4d^9 5f^2$ by only a few eV. The resonant emission is more intense than the corresponding normal emission. The numbers of elec-

trons contributing to both emissions are in the ratio 3/2 and this can explain for a large part the increase of the resonant emission intensity. For the $4d-6p$ transition, the emission probability from $U^{4+} 4d^9 5f^3$ is slightly higher than that from $U^{5+} 4d^9 5f^2$ and the ratios of spin-orbit components are the same.

III. $4d$ EMISSION SPECTRA

A. Experiment

The UO_2 samples consisted of polished plates of high purity, prepared at the Département de Thermohydraulique et de Physique du C.E.N. Grenoble. The plates were fixed with a silver glue to the water-cooled massive copper sample holder. This sample holder is the anode of an ultrahigh vacuum x-ray tube. The current density is less than 4 mA/cm^2 . No spectral change in time was observed.

The spectra were recorded by using a 50-cm-radius bent crystal vacuum spectrometer equipped with (001) TIAP slab.

TABLE V. Oscillator strengths of $3(4)d_{5/2}$, $3(4)d_{3/2}$, and $5d$ photoexcitations from $U^{4+} 5f^2 \ ^3H_4$ and characteristics of radiative recombinations from $nd^9 5f^3$.

Photoexcitation		Oscillator strengths			
		$d_{5/2}$	$d_{3/2}$	$d_{5/2}:d_{3/2}$	
$5f^2 \ ^3H_4 - 3d^9 5f^3$		0.231	0.101	2.29	
$5f^2 \ ^3H_4 - 4d^9 5f^3$		0.319	0.119	2.69	
$5f^2 \ ^3H_4 - 5d^9 5f^3$		7.840			
Radiative decay	E_{eV}	$P(10^{10} \text{ sec}^{-1})$ $d_{5/2}$	E_{eV}	$P(10^{10} \text{ sec}^{-1})$ $d_{3/2}$	$d_{5/2}:d_{3/2}$
$3d^9 5f^3 - 5f^2$	3525.1	555	3.698.9	583	0.95
$3d^9 5f^3 - 6p^5 5f^3$	3522.7	27	3689.3	46	0.6
$4d^9 5f^3 - 5f^2$	735.0	33	776.1	30	1.1
$4d^9 5f^3 - 6p^5 5f^3$	720.8	20	753.6	24	0.7
			763.3	5	
$5d^9 5f^3 - 5f^2$			15		
$5d^9 5f^3 - 6p^5 5f^3$			5		

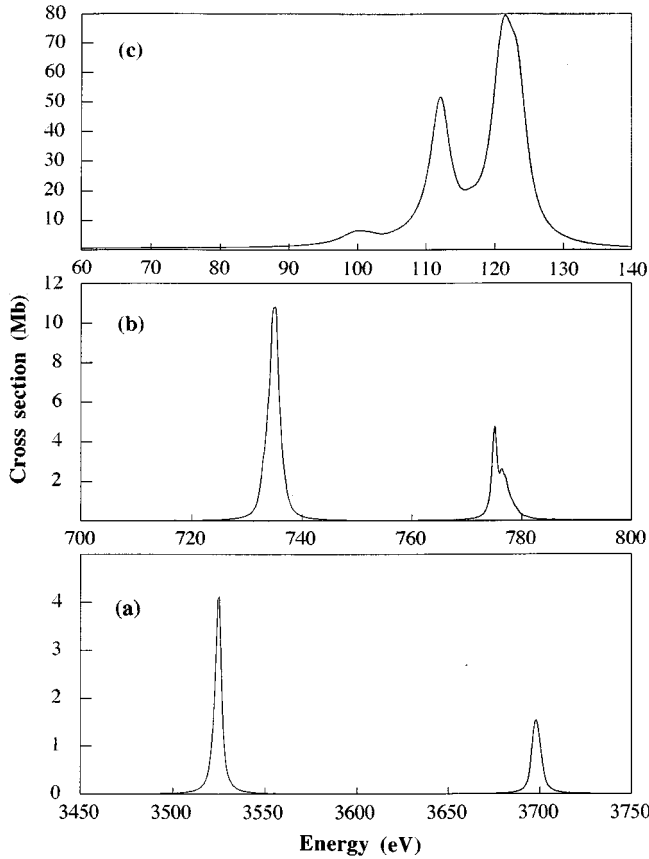


FIG. 2. U^{4+} calculated photoexcitation cross sections (Mb) from $5f^2 \ ^3H_4$ to (a) $3d^9 5f^3$ with Lorentz 3 eV wide; (b) $4d^9 5f^3$ with Lorentz 1 eV wide; (c) $5d^9 5f^3$ with Lorentz 3.4 eV wide.

A polyethylene-windowed Ar- CH_4 gas-flow proportional counter was placed behind an adjustable slit situated on the Rowland circle [27]. No impurity line was present in the relevant spectral ranges. The quasilinear background due to bremsstrahlung was subtracted.

The emissions near an excitation threshold are sensitive to self-absorption. In particular, the resonant emissions can completely disappear if the radiation path length in the sample is large. This path depends on two parameters: the orientation of the sample with respect to the observation direction, which was chosen to minimize the self-absorption and the incident electron energy E_0 , which determines the path length of the probe particles [28]. E_0 was varied from the threshold energy E_S up to $1.6 E_S$.

B. Normal $4d$ - $5p$ emission

We have chosen to analyze the normal $4d_{5/2}$ - $5p_{3/2}$ emission. It is situated at about 200 eV of the resonant emission energy range, its initial state has a $4d_{5/2}$ hole, and its transition probability is of the same order of magnitude as that of the $4d_{5/2}$ resonant emission. Moreover, as noticed in Sec. II C, there is a certain disagreement concerning the $5p_{3/2}$ subshell energy.

The spectrum observed with an incident electron energy $E_0 = 3000$ eV is plotted in Fig. 4. The maximum is situated at 546 eV with a shoulder at 543 eV. The theoretical and experimental expected emission values are 535 and 543.3 eV,

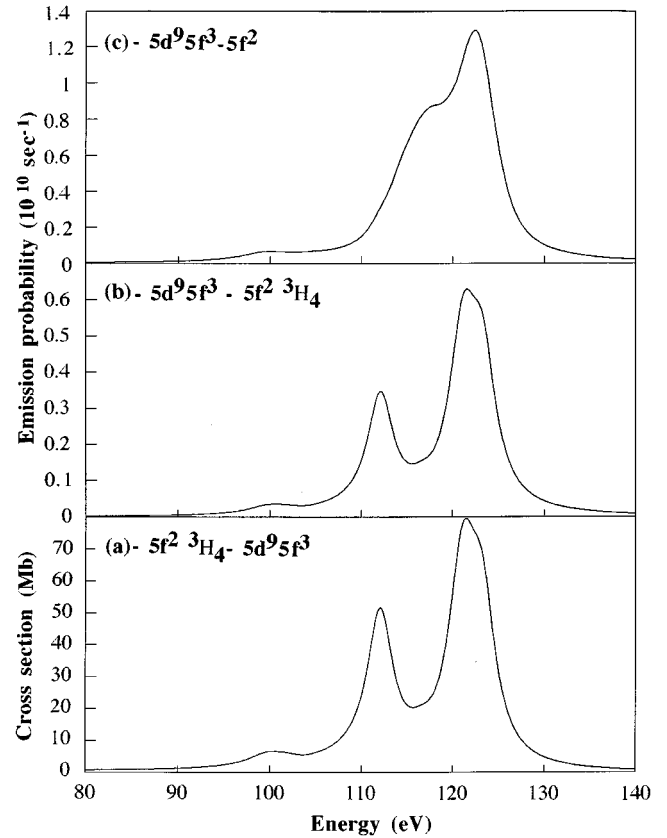


FIG. 3. Calculated spectra in the U^{4+} $5d$ range: (a) photoexcitation cross section (Mb) from the ground state; (b) resonant emission probability (10^{10} sec^{-1}) from $5d^9 5f^3$ $J=3,4,5$; (c) resonant emission probability (10^{10} sec^{-1}) from $5d^9 5f^3$.

respectively (Table II). Thus the agreement is better with the energies deduced from the experiments. This result shows that the energy calculated for $5p_{3/2}$ is too large with respect to the energies of the other subshells. This is not due to interactions with the other $5l$ subshells that are taken into account in the calculation of the ionization energies. Interaction of the $5p_{3/2}$ subshell with configurations belonging to the multiply excited or ionized U^{4+} is perhaps to be considered.

We have plotted in Fig. 4(b) the calculated spectrum shifted towards the higher energy by +12 eV to make easier the comparison between the shapes of both curves. The structures of the calculated spectrum reproduce rather well that of the experimental one. The calculated spectrum spread is about 8 eV and it is wider than the experimental one. We have verified that the large spreading of the calculated spectrum is not a lifetime effect and can be explained by the large multiplet splitting associated with the presence of the open $5f$ subshell in the free ion $U^{4+} 5f^2$. For that we have plotted the spectra obtained with Lorentz curves between 0.6 and 1 eV wide. No change of the spectrum shape is seen and the spread increase that usually accompanies a lifetime increase is negligible with respect to that due to the splitting. The experiment is made for solid oxide where the effect of multiplet splitting is expected to be smaller than for the free ion since the solid intra-atomic interactions are smaller. However the main characteristics of the normal x-ray emissions be-

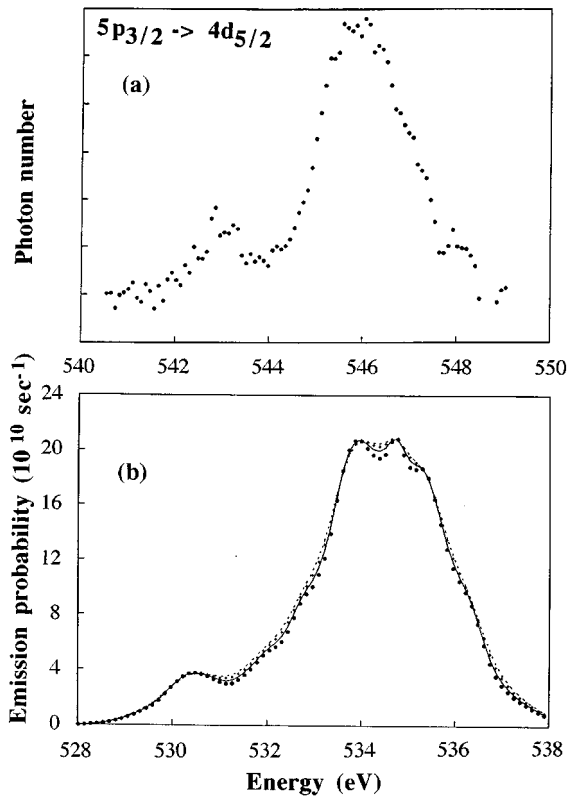


FIG. 4. U $5p_{3/2} \rightarrow 4d_{5/2}$ emission: (a) observed spectrum of UO_2 ; (b) calculated spectrum with Lorentz: 0.6 eV, full square; 0.7 eV, continuous line; 0.8 eV, dotted line; 0.9 eV, dashed line.

tween core levels observed in a solid can be described in an atomic model.

C. Emissions from the $\text{U}^{4+} 4d^9 5f^3$ excited configuration

In the U $3d$ range, we had shown that the $3d_{5/2}^5 5f^{m+1}$ excitation energy in UO_2 is close to the experimental $3d_{5/2}$ ionization energy referred to the Fermi level [11]. By analogy with this result, we expect the $4d_{5/2}^5 5f^{m+1}$ excited state in UO_2 to be situated at about 740 eV. This value is obtained by subtracting the work function (about 1–2 eV for the oxide) from the $4d_{5/2}$ ionization energy given in Table I column (5). We have analyzed the emission spectrum in the 725–755-eV range by using an incident electron energy of nominal value 745 eV. The electron kinetic energy exceeds this value by a term that depends on the characteristics of the electron beam production. This energy term is ≈ 7 eV [3] as seen in Fig. 5(a) where the radiative cutoff is observed at about 752 eV. In these conditions an emission is present at 743 eV. The spectrum observed with $E_0 \approx 1200$ eV is plotted in Fig. 5(b). The emission seen at 743 eV corresponds to that observed at the threshold and is three times more intense. A nonresolved weak structure is present at about 736 eV; its intensity is 4–5% of the main peak. An emission is observed at 762.5 eV, i.e., 19.5 eV above the main peak.

We compare the experimental emission spectra to the calculated emission and photoexcitation spectra in Fig. 5. The average energy of the $4d_{5/2}^5 5f^3 - 5f^2$ resonant emission in the U^{4+} free ion is 735.0 eV. The difference between this value and the energy of the experimental emission is 8 eV (which

is $\approx 1\%$ of the energy). The average energy of the $\text{U}^{4+} 4d_{3/2}^3 5f^3 - 6p_{1/2}^1 5f^3$ emission is 753.6 eV, i.e., 18.6 eV above the resonant emission. On the other hand, the $4d_{5/2} - 5f$ normal emission in the free ion is predicted to be 737.2 eV and the $4d_{3/2} - 6p_{1/2}$ normal emission at 757.6 eV, i.e., 20.4 eV above (Table II). Then the interpretation of the experimental emissions at 743 and 762.5 eV cannot be made from energies alone.

From the relative intensities of these two emissions and of the $4d_{5/2} - 5p_{3/2}$ normal emission, which are discussed in detail in Sec. III D, we assign the transition at 743 eV to the resonant emission $4d_{5/2}^5 5f^3 - 5f^2$ and the transition at 762.5 eV to the $4d_{3/2}^3 5f^3 - 6p_{1/2}^1 5f^3$ emission, i.e., to the $4d_{3/2} - 6p_{1/2}$ transition in the presence of the spectator excited $5f$ electron. Finally, by analogy with the $3d$ emission spectrum [11], where we had observed the $3d_{5/2} - 5f$ normal emission at about 6.5 eV towards the lower energy of the resonance emission, by increasing the incident electron energy, the structure at 736 eV is interpreted as the $4d_{5/2}^5 5f^2 - 5f^1$ emission, i.e., the $4d_{5/2} - 5f$ normal transition array.

D. Relative intensity of emissions from excited and ionized states

As already underlined, emissions from the $4d^9 5f^3$ excited states cannot be identified from their energies alone. In this section, we show that measurements of relative intensities at different incident electron energies enable us to identify emissions from different initial states.

The intensity of an x-ray emission is a function of the probability A to create the initial state, the probability P of the radiative decay from this state to the final one, the self-absorption of the radiation, and several experimental parameters. For two emissions in the same energy range, the experimental parameters, such as the response of the spectrometer, are almost the same. If the two emissions have the same initial state, their relative intensities depend on the probabilities P . Inversely, if the probabilities P are known, information can be obtained on the initial state and the probability A .

When ionized or excited initial states are produced by collision with incident electrons of energy E , their probability A depends on the ionization or excitation cross sections, $\sigma_i(E)$ or $\sigma_e(E)$, and on the incident electron energy distribution in the material. The probabilities A to create the $\text{U}^{4+} nd^{-1} 5f^{m+1}$ excited state or the $\text{U}^{5+} nd^{-1}$ ion are different and vary in a different manner with the incident electron energy E_0 . For ionization, A increases in a monotonous manner between the threshold E_S and several times E_S . For excitation, as we have shown in our experimental study of the La $3d^9 4f^1$ resonant emissions [3], the probability A has a large maximum several eV wide, situated just at the threshold. In this range, therefore, the excitation is much more probable than the ionization. Beyond it, the excitation has a small probability that increases with E in a monotonous manner up to several times E_S . This increasing can be more rapid than that for the ionization. In summary, the creation of excited states is predominant near the excitation threshold E_S .

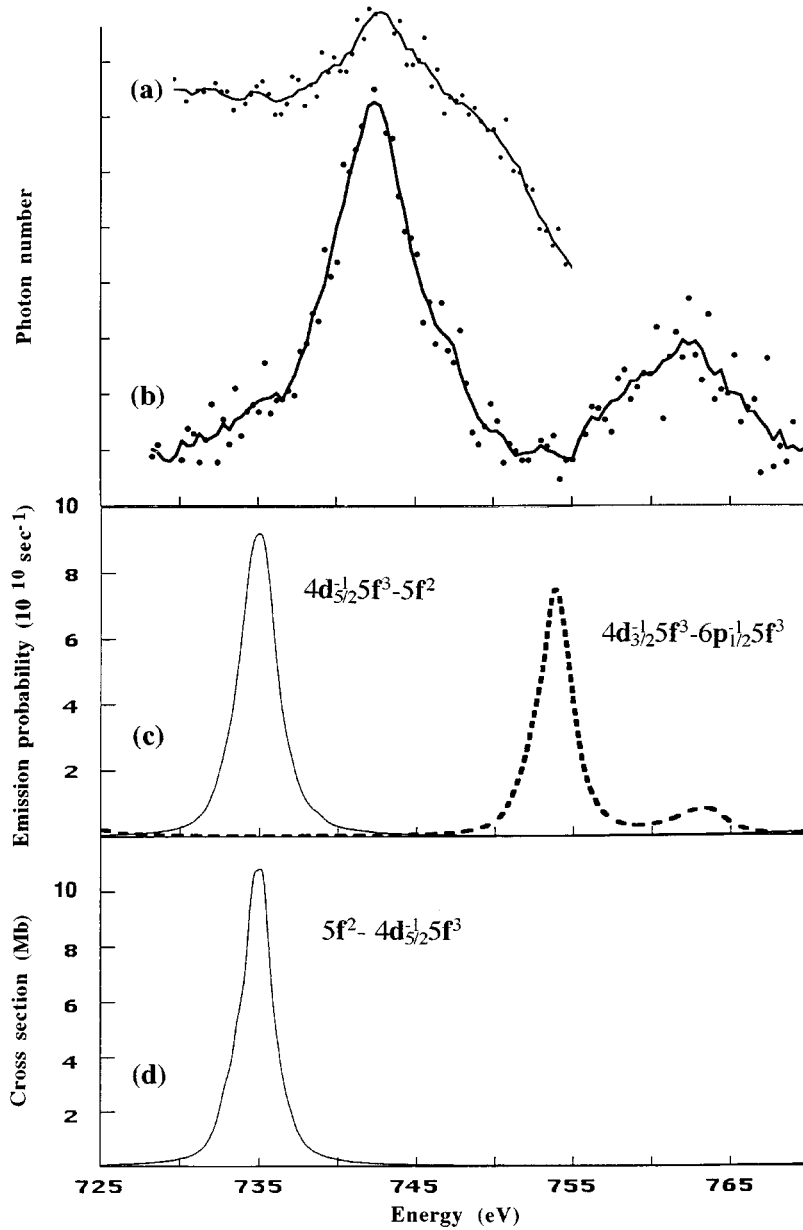


FIG. 5. U spectra in the 4d range: (a) observed emission of UO_2 at $E_0 = 745$ eV; (b) *id* at $E_0 = 1200$ eV; (c) calculated emission probability (10^{10} sec^{-1}) from $\text{U}^{4+} 4d^9 5f^3$; (d) calculated photoexcitation cross section (Mb) from $\text{U}^{4+} 5f^2 {}^3H_4$.

When the incident electrons have energy E_0 close to E_S , the thickness x in which the emission takes place (labeled emissive thickness) is small. In this small thickness, the number of electrons having the energy E_0 and the ionization and excitation cross sections, $\sigma_i(E_0)$ and $\sigma_e(E_0)$, can be considered constant. Then the number of the initial states created per area unit and time unit is

$$N_e(E_0)N_a\sigma(E_0)x,$$

where $\sigma(E_0)$ is $\sigma_i(E_0)$ or $\sigma_e(E_0)$, $N_e(E_0)$ is the number of incident electrons per area unit, and time unit, and N_a is the number of uranium atoms per volume unit. If E_0 is far from the threshold, the variation of N_e and σ_i (or σ_e) with the energy E must be taken into account and the number of initial states is a complex function of E . In the case of the ionization, semiempirical models have been established to express the relative variation of the number of the ionized states as a function of E [29].

In the energy range around 743 eV, the normal $4d_{5/2}-5f$ emission could be observed. Its transition probability is five times smaller than that of the $4d_{5/2}-5p_{3/2}$ normal emission (Table III). We have estimated that the intensity of the $4d_{5/2}$ normal emissions decreases by one to two orders of magnitude when E_0 varies from 3000 to 750 eV. Thus the $4d_{5/2}-5f$ normal emission observed at $E_0 \approx 750$ eV should be two orders of magnitude weaker than the normal $4d_{5/2}-5p_{3/2}$ emission at $E_0 = 3000$ eV while the emission observed at 743 eV is only two times weaker. Consequently the emission at 743 eV is not due to the decay of the $4d_{5/2}^{-1}$ ionized state.

We have obtained a value of 75 for the ratio of the photoexcitation and photoionization cross sections at the $4d_{5/2}$ threshold. It is known that the electron and photon interaction cross sections are proportional at a given energy in the range where the Born approximation is valid. Similarly, at the threshold, we expect that the ratio between excited and ionized states could be close to the value of 75. Then, at the

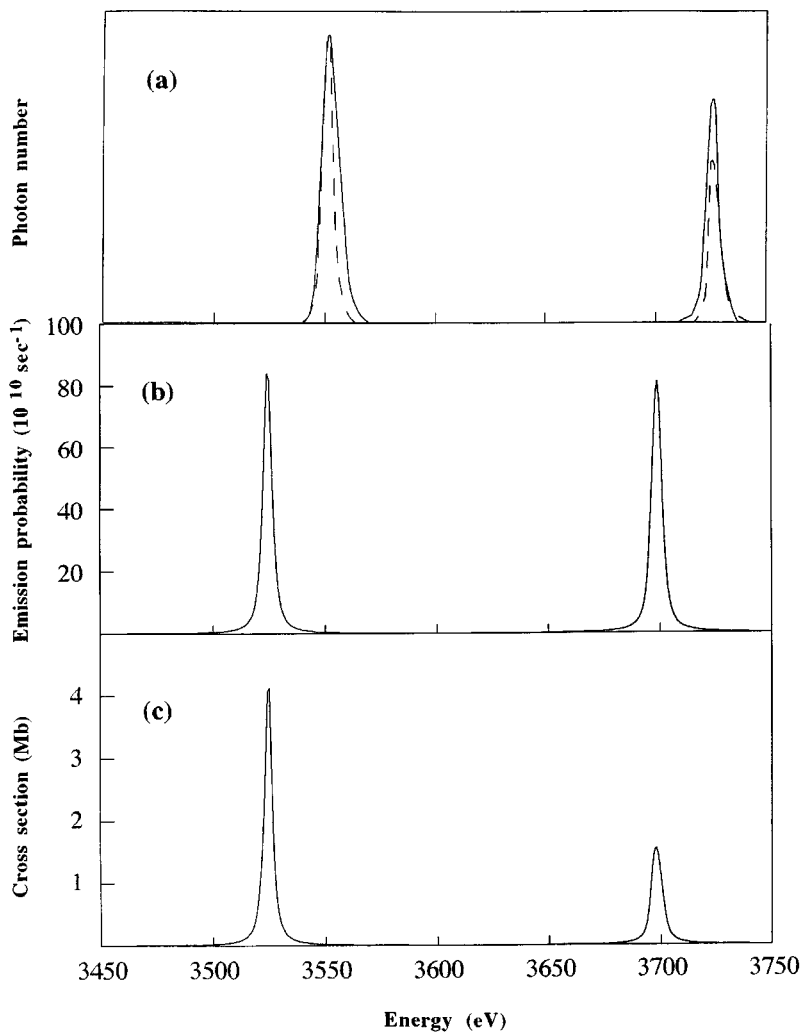


FIG. 6. U spectra in the 3d range: (a) observed emission of UO_2 at $E_0=4300$ eV [17], continuous line; observed photoabsorption [25], dashed line; (b) calculated emission probability (sec^{-1}) from $\text{U}^{4+} 3d^9 5f^3$; (c) calculated photoexcitation cross section (Mb) from $\text{U}^{4+} 5f^2 {}^3H_4$.

$\text{U } 4d_{5/2}$ threshold, the resonant emission should be about two orders of magnitude stronger than the corresponding normal emission. Consequently, we interpret the emission observed at 743 eV as the resonant emission from the $4d_{5/2}^5 5f^{m+1}$ excited configuration.

When E_0 increases [cf. Fig. 5(b)], the thickness x and the self-absorption increase and also the number of collisions. The relative number of collisions leading to the excited state with respect to that giving ionized states depends on the energy distribution of the electrons inside the material. For the lanthanides, conditions favorable to the observation of resonant emissions were obtained with E_0 between 1.2 and 1.5 E_S . Analogous results are found in the U $4d$ range.

The relative intensity of the transition observed at 762.5 eV designated as the $4d_{3/2}^3 5f^3 - 6p_{1/2}^1 5f^3$ emission, is lower in the experimental than in the calculated spectrum (cf. Fig. 5, curves b and c). The calculation takes into account only the transition probabilities P . For this emission the initial state has a $4d_{3/2}$ hole. If we assume that the probabilities A to create the excited $4d_{5/2}$ and $4d_{3/2}$ states retain the ratio of the $4d_{5/2}$ and $4d_{3/2}$ photoexcitation cross sections, i.e., 2.7 (Table V), we obtain for the intensity ratio of the two emissions 3.6, in good agreement with the experimental ratio of 3.4. On the other hand, if the probabilities A , P , and the self-absorption are taken into account, the intensity of the $4d_{5/2} - 5f$ normal emission is about 6% of that of the

$4d_{5/2}^5 5f^3 - 5f^2$ resonant emission. This confirms the interpretation proposed for the structure at 736 eV.

From relative intensity measurements, we have thus identified the transitions emitted in $nd^9 5f^{m+1}$ and nd^9 ions and justified our interpretations. These identifications are made easy by using as a probe electrons of energy close to the excitation threshold and by increasing gradually their energy. Relative numbers of each initial state can be estimated by this method.

IV. COMPARISON BETWEEN nd PHOTOEXCITATION AND RESONANT EMISSION

We have shown that emissions due to the decay of the $4d^9 5f^{m+1}$ excited states created under electron bombardment, i.e., resonant emission and emission in the presence of the spectator electron, are observed in the oxide UO_2 . The $3d_{5/2}$ and $3d_{3/2}$ resonant emissions had been identified in the emission spectrum of UO_2 [11,12]. In the $5d$ range, large oscillator strength is known to be present and forms the so-called "giant" resonance [30]. The radiative decay of corresponding excited states had been observed in U_3O_8 and attributed to an atomic bremsstrahlung effect [13]. In Sec. II, we have calculated the photoexcitation and the resonant emissions by using the same theoretical model in the three

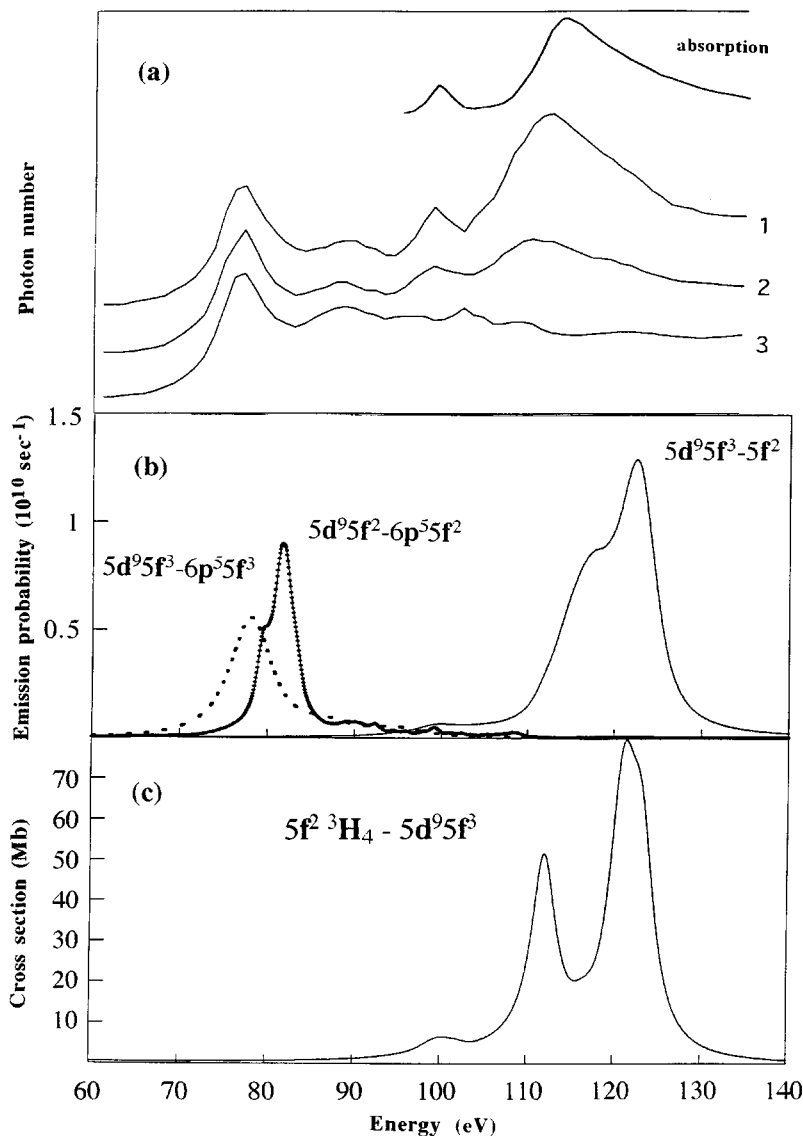


FIG. 7. U spectra in the 5*d* range: (a) observed emission of UO_2 : (1) at $E_0 = 500$, (2) at 1500, (3) at 4000 eV [18]; observed absorption [18] (b) calculated emission probability (10^{10} sec^{-1}) of U^{4+} resonance emission, $\text{U}^{4+} 5d^9 5f^3 - 6p^5 5f^3$ and $\text{U}^{5+} 5d^9 5f^2 - 6p^5 5f^2$; (c) calculated photoexcitation cross section (Mb) from $\text{U}^{4+} 5f^2 \ ^3H_4$.

nd ranges in order to compare the simulated spectra to the experimental ones.

Comparison in the 3*d* range is plotted in Fig. 6. The UO_2 3*d* photoabsorption and resonant emission excited with incident electron energy of 4.3 keV [12] are plotted in Fig. 6(a) and the calculated emission and photoexcitation spectra in Figs. 6(b) and 6(c). The experimental conditions are such that spectral perturbations due to the absorber thickness, to the self-absorption, etc., are very low. Resonant emissions had been identified by comparing the emission and photoexcitation spectra whose maxima were observed at the same energy (with an experimental precision ≈ 0.5 eV) [12]. Calculated resonant emission and photoexcitation maxima are also at the same energy. Observed and calculated emissions are in agreement, in particular, the ratio of the $3d_{5/2}$ to $3d_{3/2}$ components. This ratio is expected to be higher in photoexcitation, in agreement with the experiment. The shape of spectra is governed by the multiplet splitting. As in the 4*d* range, the excitation energies calculated for the U^{4+} free ion are lower than the experimental value obtained for solid UO_2 . The difference is about 25 eV (which is 0.7% of the energy).

The results concerning the 5*d* range are plotted in Fig. 7. Comparison between the simulated spectra and the ones observed for U_3O_8 is difficult because the latter were perturbed by the choice of the experimental conditions. For absorption, the absorber was a few ten nm thick whereas its thickness could not exceed 5 nm [28]. For resonant emission, the incident electron energy was $4E_S$, $12.5E_S$, or $33E_S$ (where E_S is the threshold energy), leading to strong self-absorption effects. Spectral perturbations change the relative heights of the peaks and introduce broadenings that modify strongly the shape of the spectra. Moreover, the shape of the calculated spectra is very sensitive to the configuration of uranium, which is not purely $5f^2$ in U_3O_8 . There is, however, a general agreement between the observed and calculated spectra, in particular the relative importance of the peak at 100 eV with respect to the main peak. Concerning the emission at 80 eV, taking into account its relative intensity with respect to the peak at 100 eV, we suggest that it is due to the $5d-6p$ transitions in the presence of the spectator excited $5f$ electron.

The same theoretical model accounts for the experimental results in the three energy ranges. This shows that the model

is suitable for describing the U x -ray transitions in the $3d$, $4d$, and $5d$ ranges and that the characteristics of the U nd excited states are similar in spite of large differences in the shape of the spectra. These differences are due to the evolution from the jj coupling valid for the $3d$ and $4d$ orbitals to complex scheme for the $5d$ shell.

In summary, information on the dynamics and the localization of high-energy states created by electron or photon interactions can be obtained from the analysis of their decay processes in a time scale, which is a function of the core hole lifetime, i.e., of the order of 10^{-14} – 10^{-16} s. As has already been pointed out, in the case of excited states produced by collisional excitation, no interference exists between excitation and decay processes. One can get experimental conditions such that excited states are created preferentially with all their J levels statistically populated. Under these condi-

tions, radiative and nonradiative direct recombinations and transitions in the presence of the spectator excited electron are observed simultaneously from the whole excited configuration. The study of excited states by x -ray emission stimulated by threshold energy electrons can be generalized to states of any symmetry and more complex systems because of the local character of the radiative transitions involving an inner subshell.

ACKNOWLEDGMENTS

The authors thank Dr. Ph. Dehaut of C. E. N. Grenoble who has provided us with the samples. They are grateful to Dr. N. Spector for critical reading of the manuscript. They acknowledge the IDRIS, Centre National de la Recherche Scientifique, for computer facilities.

-
- [1] C. Bonnelle and R. C. Karnatak, C. R. Acad. Sci. Paris **268**, 494 (1969); J. Phys. **32**, C4-230 (1971).
- [2] G. Dufour and C. Bonnelle, J. Phys. (Paris) **35**, L255 (1974).
- [3] T. Aberg and J. Tulkki, in *Atomic Inner-Shell Physics*, edited by B. Crasemann (Plenum, New York, 1985), Chap. 10.
- [4] C. Bonnelle, in *Advances in X-ray Spectroscopy*, edited by C. Bonnelle and C. Mandé (Pergamon, Oxford, 1982).
- [5] C. Bonnelle, in *X-ray and Inner-shell Processes in Atoms, Molecules and Solids*, edited by A. Meisel and J. Finster (Karl-Marx-Universität, Leipzig, 1984), p. 317.
- [6] P. Motais, E. Belin, and C. Bonnelle, Phys. Rev. B **30**, 4399 (1984).
- [7] T. M. Zimkina, A. S. Shulakov, V. A. Fomichev, A. P. Braiko, and A. P. Stepanev, in *X-ray and Inner-shell Processes in Atoms, Molecules and Solids*, edited by A. Meisel and J. Finster (Karl-Marx-Universität, Leipzig, 1984), p. 263.
- [8] K. Ichikawa, A. Nisawa, and K. Tsutsumi, Phys. Rev. B **34**, 6690 (1986).
- [9] G. Dufour, R. C. Karnatak, J. M. Mariot, and C. Bonnelle, J. Phys. (Paris) **37**, L119 (1976).
- [10] F. Gerken, J. Barth, K. L. I. Kobayashi, and C. Kunz, Solid State Commun. **35**, 179 (1980).
- [11] J. C. Riviere, F. P. Netzer, G. Rosina, G. Strasser, and J. A. D. Matthews, J. Electron Spectrosc. Relat. Phenom. **36**, 331 (1985).
- [12] M. Richter, T. Prescher, M. Meyer, E. v. Raven, B. Sonntag, H. E. Wetzel, and S. Aksela, Phys. Rev. B **38**, 1763 (1988).
- [13] C. Bonnelle, G. Giorgi, and J. Bruneau, Phys. Rev. B **50**, 16 255 (1994).
- [14] J. L. Dehmer, A. F. Starace, U. Fano, J. Sugar, and J. W. Cooper, Phys. Rev. Lett. **26**, 1521 (1971).
- [15] J. Sugar, Phys. Rev. B **5**, 1785 (1972).
- [16] C. Bonnelle and G. Lachéré, J. Phys. (Paris) **35**, 295 (1974); C. Bonnelle and G. Lachéré, in *Plutonium and Other Actinides*, edited by H. Blank and R. Lindner (North-Holland, Amsterdam, 1976).
- [17] C. Bonnelle, Struc. Bonding **31**, 23 (1976).
- [18] T. M. Zimkina, A. S. Shulakov, and A. P. Braiko, Fiz. Tverd Tela Leningrad **23**, 2006 (1981) [Sov. Phys. Solid State **23**, 1171 (1981)].
- [19] J. Bruneau, J. Phys. B **16**, 4135 (1983).
- [20] S. J. Rose, N. D. C. Pyper, and I. P. Grant, J. Phys. B **11**, 755 (1978).
- [21] J. P. Desclaux, At. Data Nucl. Data Tables **12**, 311 (1973).
- [22] K. Siegbahn, C. Nordling, A. Fahlman, and K. Hamrin, Nova Acta Regiae Soc. Sci. Ups. **XX**, 11 (1967).
- [23] Y. Cauchois, J. Phys. Radium **13**, 113 (1952).
- [24] G. Lachéré, C. R. Acad. Sci. Paris **267**, 821 (1968); C. Bonnelle and G. Lachéré (unpublished).
- [25] Y. Cauchois, C. Bonnelle, and I. Manescu, C. R. Acad. Sci. Paris **267**, 817 (1968).
- [26] J. C. Fuggle, A. F. Burr, L. M. Watson, D. J. Fabian, and W. Lang, J. Phys. F **4**, 335 (1974).
- [27] C. Bonnelle, F. Vergand, P. Jonnard, J.-M. André, P.-F. Staub, P. Avila, P. Chargelègue, M. F. Fontaine, D. Laporte, P. Paquier, A. Ringuenet, and B. Rodriguez, Rev. Sci. Instrum. **65**, 3466 (1994).
- [28] C. Bonnelle, R. Soc. Chem. Annu. Rep. C **1987**, 201 (1987).
- [29] P.-F. Staub, J. Phys. D **27**, 1533 (1994); **28**, 252 (1995); x -ray Spectrom. (to be published).
- [30] G. Wendin and N. Kerr Del Grande, Phys. Scri. **32**, 286 (1985).